PCCP

Accepted Manuscript

This is an *Accepted Manuscript*, which has been through the Royal Society of Chemistry peer review process and has been accepted for publication.

Accepted Manuscripts are published online shortly after acceptance, before technical editing, formatting and proof reading. Using this free service, authors can make their results available to the community, in citable form, before we publish the edited article. We will replace this *Accepted Manuscript* with the edited and formatted *Advance Article* as soon as it is available.

You can find more information about *Accepted Manuscripts* in the Information for Authors.

Please note that technical editing may introduce minor changes to the text and/or graphics, which may alter content. The journal's standard Terms & Conditions and the Ethical guidelines still apply. In no event shall the Royal Society of Chemistry be held responsible for any errors or omissions in this *Accepted Manuscript* or any consequences arising from the use of any information it contains.

ROYAL SOCIETY OF CHEMISTRY

www.rsc.org/pccp

Dynamic Article Links ▶

PCCP

Cite this: DOI: 10.1039/c0xx00000x

www.rsc.org/xxxxxx

Paper

Tailoring of carbon nanowall microstructure by sharp variation of plasma radical composition

Kirill V. Mironovich,[a] Daniil M. Itkis,[b,c] Dmitry A. Semenenko,[b] Sarkis A. Dagesian,[d] Lada V. Yashina,[b] Elmar Yu. Kataev,[c] Yuri A. Mankelevich,[a] Nikolay V. Suetin,[a,e] and Victor A. Krivchenko*[a,b]

Received (in XXX, XXX) XthXXXXXXXXX 20XX, Accepted Xth XXXXXXXXX 20XX

DOI: 10.1039/b000000x

In this paper we propose new and simple method to tune carbon nanowall microstructure by sharp variation of CH_4/H_2 plasma conditions. Using theoretical calculations we demonstrated that the sharp variation of gas pressure and discharge current leads to significant variation of plasma radical composition. In some cases such perturbation creates the necessary conditions for the nucleation of smaller secondary nanowalls on the surface of primary ones.

1 Introduction

Carbon nanowall (CNW) films are composed of dense arrays of micron-sized flakes of multilayer graphene (or graphite), which have dominating vertical orientation and chaotic lateral distribution with hundreds of nanometers spacing between neighbouring walls. Flake thickness varies from several graphene layers to tens of nanometers. Such materials were already suggested for various applications such as electron field emitters,[1,2] catalyst supports[3], templates for nanostructured material synthesis[4,5], black body anti-reflective coatings[6] and others.

The CNW films formation was firstly observed during microwave plasma enhanced chemical vapor deposition (PECVD) from $CH_4$and H_2 precursor mixtures[7]. Different ways of plasma activation[8] as well as different carbon precursors (including natural ones, e.g. honey)[9,10] were employed from that time in order to grow wall-like carbon structures on various kinds of substrates. It was demonstrated that the film growth starts with plasma etching of the surface with simultaneous production of thin carbon sub-layer in the very beginning of discharge ignition[11-13]. Afterwards plasma parameters are smoothly changed from discharge breakdown conditions, which are reached at high applied voltages and/or low gas pressure, to steady-state that is maintained during further carbon film nucleation and linear growth[11].

While mechanisms of nucleation and growth of carbon nanowall films and sparse vertical graphene sheets are studied to a certain extent,[9,14-16] there is still no clue about the mechanisms driving microstructural evolution in such kind of materials, especially for the cases when the film synthesis proceeds for extended times or the film undergoes an additional treatment, which results in various complex nanostructures formed on CNW surface[11,17]. The comprehensive studies of the pathways underlying the processes of interest require simultaneous *in situ* monitoring of a large variety of radicals that exist in CH_4/H_2 plasma as they all contribute to nucleation and growth of the final carbon coatings. However, no single tool can be found for such observations. E.g. optical emission spectroscopy can be suitable for detection of radicals with permitted optical transitions only (i.e. C_2 or CH), while most of radicals, for instance CH_3, have only forbidden transitions[18] thus its detection requires mass spectroscopy or optical absorption spectroscopy in UV range (e.g. cavity ring down spectroscopy method[19]). The need for advanced characterization techniques significantly hinders the research focused on CNW architecture formation mechanisms, while the lack of fundamental understanding prevents an effective control of coating morphology and functional parameters, including specific surface area, anisotropy, optical properties and others.

Here we study evolution of the CNW film microstructure during PECVD growth involving rapid variation of operational parameters. We employed a two dimensional plasma theoretical model[20,21] and show that rapid change in discharge current and gas pressure can be used for fine tuning of the plasma composition that in turn allows to control the rates of the CNW growth, hydrogen etching of its surface and defect healing. We found that fast rise in glow discharge current leads to a remarkable increase in the concentrations of alkyl radicals (C_xH_y). These radicals may chemisorb on basal planes of growing CNWs thus promoting secondary nucleation and deposition of new smaller flakes right on the surface of primary ones. Such approach provides a tool to precisely control specific surface area of CNW coatings and can be used for fine tuning of its microstructure.

2 Experimental section

The CNW films were grown on silicon substrates in the plasma of direct current (dc) glow discharge in a mixture of methane and hydrogen. At the start of the process reactor was

Physical Chemistry Chemical Physics Accepted Manuscript

filled with hydrogen. The gas pressure was maintained at 20 Torr at the moment of discharge ignition and then gradually increased up to 60Torr. Simultaneously discharge current was raised up to 0.7 A. Hydrogen flow rate was kept at 10 l/h value. Then methane was introduced at flow rate of 1 l/h and total gas mixture pressure increased up to 150 Torr. In all experiments duration of a CNW film growth was measured from the methane supply start and was equal to 25 minutes. Standard regime of the film growth corresponded to discharge current of 0.7 A, pressure of working gas mixture of 150 Torr, H_2/CH_4 flow rates of 10 and 1 l/h, respectively. A part of the samples were synthesized with a similar procedure, but involving sharp change (in less than 5 seconds) of discharge current (from 0.7 to 0.9 A, marked as S0-S1 in Fig. 1), system pressure (from 150 to 100 Torr, marked as S0-S2 in Fig. 1) or both (marked as S0-S3 in Fig. 1) after 20 minutes of growth. Our estimations reveal that after such rapid change all plasma parameters achieve quasi-stationary stage during less than 1 minute. Table summarizing experimental synthesis parameters can be found in Supplementary Information (Table T1).

SEM images were obtained using Carl Zeiss Supra 40 microscope with field emission cathode. JEOL JEM 2100F high-resolution microscope operating at 200 kV accelerating voltage was employed for TEM observations. Raman spectra were collected using Renishaw in Via Raman microscope. Ar^+ laser (514 nm wavelength), focused on the sample using 50x lens in a spot of 5μm in diameter, was used as an excitation source.

C1s X-ray absorption spectra were recorded at RGBL beam line of Hetlmholtz Zentrum Berlin, BESSY II synchrotron facility (Germany) with 0.05 eV step. Collected data were normalized to X-ray flux, background was subtracted using arctangent step-like function with exponential decay.

For double electric layer capacitance measurements the working electrodes were prepared by growing a CNW films on stainless steel foil using the same plasma conditions. The counter electrode was prepared by mixing 90 % of carbon black Super C65 (Timcal) and 10% of polyvinylidene fluoride (Solef 5130, Solvay) in N-methyl-2-pyrrolidone (BASF) and coating of resulting slurry on Al foil. Both electrodes were dried in a vacuum oven at 120°C for 12 hours before use. Pouch-type supercapacitors were assembled in an Ar-filled glove box (Labconco Protector CA). 1M solution of 1-ethyl-3-methylimidazolium tetrafluoroborate ($EMIMBF_4$, Aldrich) in anhydrous acetonitrile (Aldrich) was used as electrolyte. Cyclic voltammograms were recorded with a Biologic SAS SP-300 potentiostat at 100 mV/s voltage sweep rate.

Simulation of radical composition in the plasma was performed using two dimensional model[20,21].The set of non-stationary conservation equations for mass, momentum, energy and species concentrations was implemented as a finite difference approximation. The electric field distribution was determined by current conservation equation *div*(*j*)=0 simultaneously with conservation equations for charged particles. Rate coefficients for electron-particle reactions where determined from electron energy distribution function calculated by solving the Boltzmann equation in a two-term approximation[21]. Validation of the model has been made by comparison of calculated discharge parameters with parameters measured during experiment (for instance voltage). Volume of the plasma was calculated in accordance with spatial distribution of H_α line in discharge gap. Image of discharge gap with ignited plasma is presented in Fig.S1 in Supplementary Information.

3 Results and discussion

For a given DC PECVD processes operation parameters that can be used to control film growth are normally discharge current, overall pressure inside the chamber, gas composition and flow rate. The substrate temperature achieved during growth process is determined by a combination of these parameters. As it is a discharge current and pressure that cause a relatively fast response we used these two parameters to control the CNW morphology.

Standard growth process occurs with operating parameters stabilized at a certain level[1,11] (Fig. 1a) and results in uniform CNW coverage with a mean height of 3.8±0.35 µm (Fig.1b,c). Single CNWs comprise of 8– 15 graphene layers (Fig. 1b-inset) and are vertically aligned with a random orientation. In the vicinity of the substrate CNW basal planes contain etch pits (Fig. 1c, for more details see Fig.S2b), which might be associated with etching of the graphitic surface by hydrogen-containing plasma.

Recently we demonstrated that during DC PECVD process carbon nanowall edges may act as nucleation sites for cone-shaped carbon nanotubes[11]. However effective catalyst-free growth of such nanotubes requires substrate temperatures above 1000°C[1], while at the relatively low temperatures, which were achieved in this work, the amount of nanotubes was negligible.

Surprisingly, we found that the rapid rise of discharge current from 0.7 to 0.9 A (within several seconds) and maintaining this value for the last 5 minutes of overall growth period (Fig.1d) lead to a drastic change in the film morphology, which is revealed in Fig.1e,f. In addition to further growth of primary CNWs smaller nanowalls are formed on primary CNW faces that might indicate that secondary nucleation intensified as current change was applied. Interestingly, SEM study of the samples prepared by such two-step process didn't reveal any etch pits.

At lower pressure in the system hydrogen etching is significantly intensified. We found that the rapid pressure drop from 150 to 100 Torr performed after 20-minute deposition (Fig. 1g) leads to much higher concentration of etch pits on the CNW surface even after 5-minute exposure to a reduced pressure (Fig. 1h, close-ups can be found in Supplementary Information, Fig.S2c). At the same time comparison of the mean CNW height, measured after 20-minute deposition (2.4 ±0.3 µm), with the final value of 2.8 ±0.33 µm (Fig. 1i) demonstrates that the CNW growth rate was rather small at reduced pressure, giving us a hint that hydrogen etching is prevailing process in this case.

Although the evolution of the films microstructure is easily seen in all the described cases, jumps of either discharge current or pressure lead to simultaneous change of substrate temperature making it hard to filter its effect out. While pressure drop results in substrate temperature decrease from 720 to 650°C (Fig. 1d), rapid rise of discharge current leads to substrate heating up to 790°C (Fig. 1h). Fortunately, synchronized change of both parameters allows keeping the substrate temperature at nearly constant level of 720°C (Fig. 1k) thus making it easier to distinguish between the effects of temperature, pressure and

Physical Chemistry Chemical Physics Accepted Manuscript

This journal is © The Royal Society of Chemistry [year]

discharge current. The resulting mean CNW height in this case is 3.1 ±0.37 μm and the film appears to contain features observed in both previous cases giving a hint that temperature, which was nearly constant, is not directly responsible for the morphology changes. Thus we believe that rapid rise of discharge current leads to nucleation of secondary nanowalls remarkably increasing CNW coating surface area.

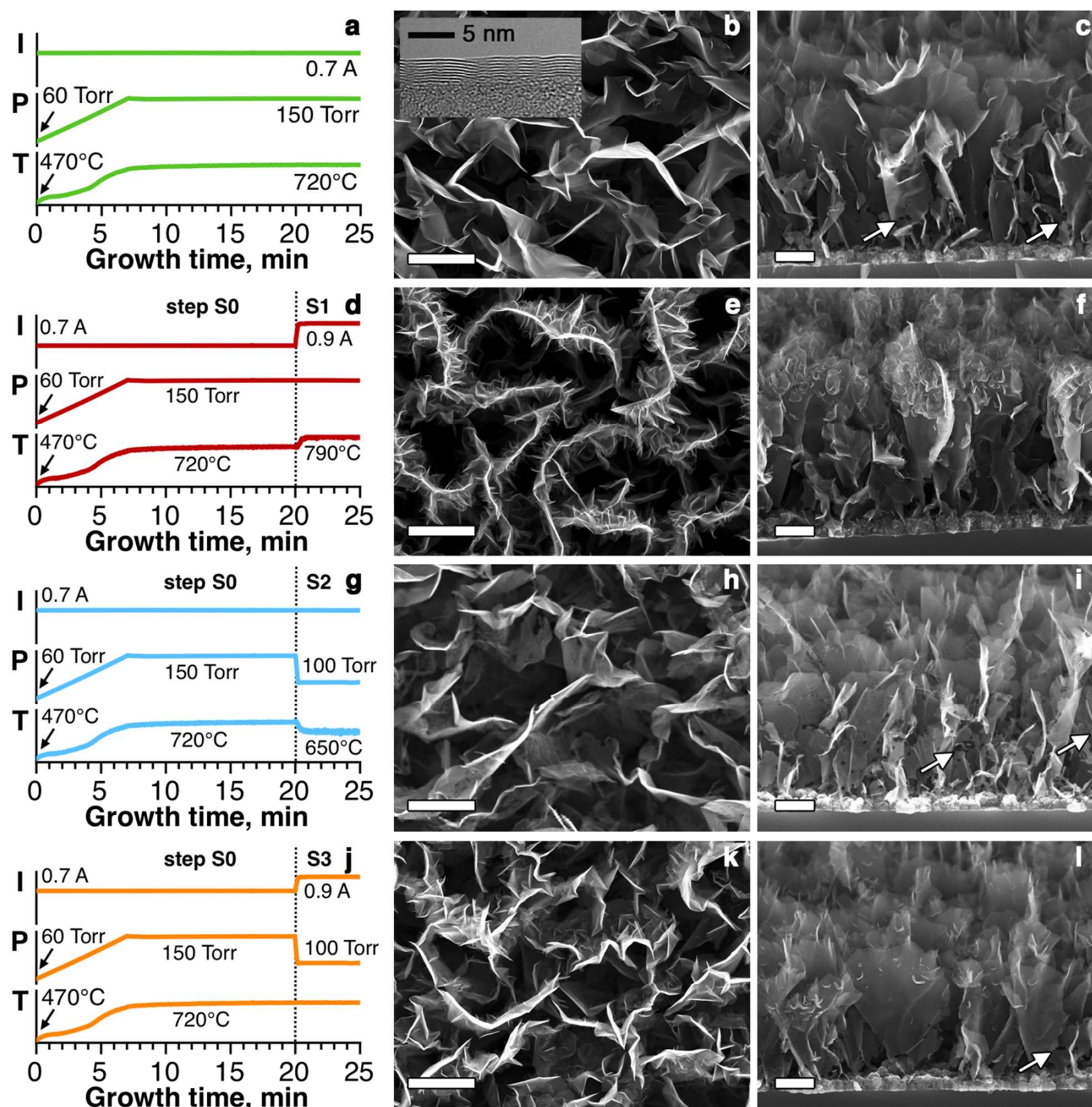

Figure 1. Synthesis regimes (a, d, g, j), top-view (b, e, h, k) and side-view (c, f, i, l) SEM images of the corresponding CNW samples. Scale bars are 1 μm. Arrows denote etch pits

To further support microscopic observations we employ electrochemical measurements in order to evaluate the integral surface area changes. Cyclic voltammetry of CNW working electrodes in acetonitrile-based electrolyte demonstrated that electric double layer capacity increases (Fig.2a) by more than 2 times (425 $\mu F/cm^2_{geom}$ in comparison to 200 $\mu F/cm^2_{geom}$) for the sample where secondary nanowalls are formed due to discharge current jump. That indicates a significant enhancement of specific surface by secondary nanowalls and agrees with microscopy data.

We further characterize structural properties of carbon films and show that different defects are generated in the CNW films in cases of sharp change of pressure or discharge current. As expected, all CNW samples possess graphitic structure with high degree of perfection that is confirmed by both near-edge X-ray absorption spectroscopy (NEXAFS) and Raman scattering (Fig.2b,c). NEXAFS spectra of all samples reveal all features typical for graphite.

Physical Chemistry Chemical Physics Accepted Manuscript

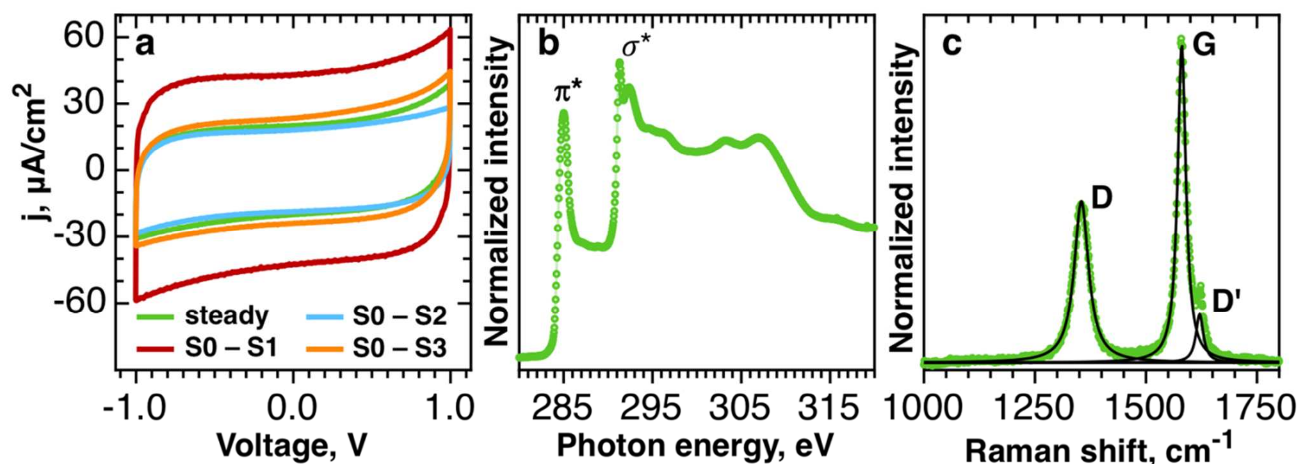

Figure 2. (a) Cyclic voltammograms recoded in two-electrode cells with the CNW electrode. 1 M solution of EMIM BF_4 in acetonitrile was used as electrolyte, sweep rate is 100 mV/s. (b) NEXAFS spectrum of CNWs, which were grown at steady plasma conditions (regime S0-S0, Figure 1a), recorded at X-ray incidence angle θ=45°. (c) Raman spectrum of the same CNW film. Experimental data is shown as points; solid lines denote components fit.

A Raman spectrum typical for the CNW samples is presented in Fig. 2c. The region of 1200 – 3200 cm^{-1} includes all main peaks characterizing graphite-like materials[22]. Based on spectra deconvolution, intensity ratios between main components were calculated and summarized in Table 1 for the samples, synthesized in different regimes (detailed spectra can be found in Supplementary Information, Fig. S3).

Analysis of D-to-G mode intensity ratio (I_D/I_G) reveals that rapid rise of discharge current, which leads to secondary nanowall nucleation and growth, results simultaneously in a remarkable defects production. I_D/I_G parameter, which is increased from 0.51 for "standard" CNWs to 1.36 for the sample prepared following S0-S1 (Fig.1d,f) or to 0.97 for the sample characterized by lower secondary nanowall amount (S0-S3 regime, Fig.1k,l), manifests that secondary nucleation is associated with appearance of additional defect sites[22]. $I_D/I_{D'}$ ratio, known to be non-sensitive to defect concentration but indicative for its type[23,24], is estimated to be about 2.8 for those samples. Such $I_D/I_{D'}$ value is typical for defects associated with presence of flake edges[23] and explains the observed trend of I_D/I_G increase for the samples where SCNWs were formed and thus new boundaries appeared. It is worth noting that the sample, which was exposed to the system pressure drop (Fig.1g,l) and exhibited a significant amount of etch pits on a CNW surface, has $I_D/I_{D'}$ of roughly 3.7 giving an evidence that point defects prevail as we can expect in case of hydrogen etching of a CNW surface.

Table 1. Results of Raman spectra deconvolution for the CNW films grown in different regimes.

	Synthetic regimes			
	S0 – S0	S0 – S1	S0 – S2	S0 – S3
ID/IG	0.51	1.36	0.65	0.97
ID/ID'	2.9	2.8	3.7	2.8

To shed the light on possible mechanisms of the CNW structure and defect evolution we analyzed radical composition in H_2/CH_4 plasma by employing the well-established two dimensional $2D(r,z)$ model, which considers reactions between 32 neutral and charged species. All considered reactions are summarized in Table T2 in Supplementary Information. We assumed that carbon nanowall growth is controlled by neutral C_xH_y radicals, since the substrate is placed on anode in our case. Also we assumed that at each step of synthesis stationary plasma conditions were quickly achieved, and evaluated radical concentration for different synthesis parameters (Table 2).

Calculations show that sharp increase in discharge current (regime S0 – S1, Fig.1d) leads to an increment in atomic hydrogen, C and CH, CH_2, C_2H, C_3, C_3H radical concentrations. Although the calculated concentration of CH_3 species, which were recently demonstrated to be the main building blocks in CNW formation[11], is reduced after the jump of the discharge current, we observe the film growth with nearly constant rate (0.32μm/min in comparison with 0.28μm/min, detected at lower current). It might be connected with intensified participation of other neutral radicals found near anode (C, CH, CH_2, C_2H, C_3, C_3H) in growth events together with CH_3 species. However, the kinetics is believed to be quite different for various radicals that most probably leads to decrease in a CNW crystallinity and microstructure distortion. While radical incorporation to CNW edges drives its further vertical growth, C_xH_y trapped on CNW basal planes form fragments of defect graphene layer, which covers the primary CNW surface non-uniformly. It's worth noting that C_xH_y (x=1, 2 and y=1, 2, 3) can be chemisorbed even at defectless basal planes and according to theoretical estimations energy benefit is in a reasonable range of 0.9 – 2.0 eV[25]. Lateral growth of the defect graphene islands can lead to either its overlapping with further secondary nanowall formation, or to a deviation from primary growth direction after another defect is being met (Fig. 3 and Supplementary Information, Fig. S4). Finally, the upper part of the CNWs (Fig. 1f), is being covered with a plenty of small secondary nanowalls during last 5 minutes at increased discharge current, which altered plasma composition.

This journal is © The Royal Society of Chemistry [year]
Physical Chemistry Chemical Physics Accepted Manuscript

Another possible reason for preservation of the film growth rate and as well for the growth of secondary nanowalls even after CH_3 radical concentration drop might be linked with slowing of hydrogen etching that is more intense at temperatures between 300 and 600°C[26]. As the quick lift of the plasma discharge current causes additional heating of the substrate from 720 to 790°C (Fig.1d) we can assume that the rate of the CNW etching, which starts from adsorption of atomic hydrogen and proceeds with consecutive formation of –CH, –CH_2, –CH_3 and free CH_4 molecule[27], is lower.

Interestingly, the etch pits could be hardly detected for the films grown at increased discharge current, while such defects are clearly seen after first 20 minutes of "standard" synthesis (see Supporting Information). Recently it was shown theoretically that during PECVD process CH_x radicals (where x=1, 2, 3) may interact with graphene surface that results in healing of single vacancy defects.[28] The authors proposed that this process includes chemisorption of CH_x species followed by carbon incorporation into the defective graphene and desorption of hydrogen. The overall reactions are barrierless and exothermic and thus their rate predominantly depends on the plasma composition. Our calculations reveal increased CH and CH_2 radical concentrations relative to atomic hydrogen, thus we believe that defect healing is promoted.

Another way to control plasma content is a variation of total pressure. Drop of the total pressure (process S0–S2, Fig. 1g,i) results in numerous etch pits easily identified on a carbon nanowall surface, which are the results of intensified hydrogen etching. Additional experiment on hydrogen plasma treatment of "standard" carbon nanowall film supports this assumption and was found to lead to significant etching of a CNW surface and to destruction of its crystal structure (Fig. S5 in Supplementary Information). Growth rate is also decreased upon pressure drop from 280 to 85 nm/min in spite of the significant increment in CH_3 concentration (see Table 1). We associate this observation with significant decrease in substrate temperature (from 720 to 650°C), which was demonstrated to control etching rate. We also assume that defect healing is significantly inhibited due to decreased concentrations of some C_xH_y radicals.

As expected simultaneous changes in discharge current and pressure, which allow keeping the substrate temperature constant (process S0–S3, Fig. 1j,l), do not cause significant etching of the CNW basal plane, which confirms that the temperature controls etching rate in hydrogen-containing plasma. Secondary nanowalls are also being produced for such samples, however its amount is much lower in comparison with synthesis at increased discharge current. This also indicates the role of both C_xH_y radicals and temperature in secondary nanowall nucleation.

Interestingly that the most etched regions are located at the bottom of the CNWs. We associate it with loss of radicals on the film surface (or upper region) and variation of C_xH_y concentration with the film thickness. A CNW film grows under continuous flux of C_xH_y radicals from plasma. Part of these radicals loss on the film surface via incorporation to graphene edges and the secondary nanowall formation. As a consequence region near a CNW bottom may be enriched with hydrogen and thus etching processes are more intense.

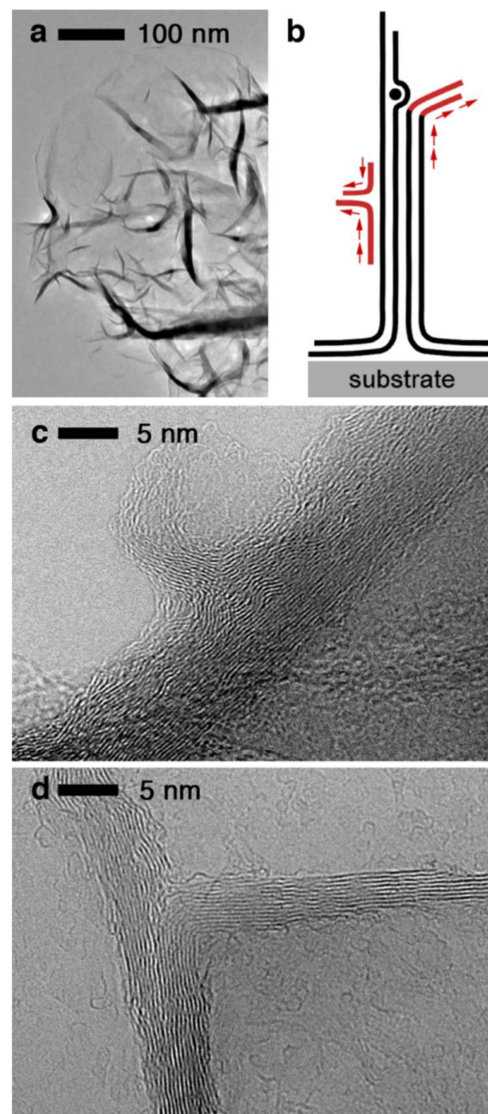

Figure 3. Low- (a) and high- (c, d) magnification TEM images of the secondary nanowalls on the CNW surface. Sketch (b) illustrates possible mechanisms of the secondary nanowall formation, arrows indicate direction of growth.

Finally it should be noted that our calculations revealed presence of C_3 and C_3H radicals. Role of these radicals is not considered in the frames of this work since their interaction with graphene-like structures is not yet understood and should be separately studied. The same applies to C_2 radicals, which are much more often discussed in literature as they are easily observed in plasma optical emission spectra (see Fig. S6). Our simulations revealed almost one order of magnitude lower concentration of C_2 radicals in comparison with concentrations of other hydrocarbon species in the plasma of dc glow discharge. Moreover C_2 concentration seriously drops above the substrate (four orders of magnitude) in comparison with C_2 concentration at the plasma center where gas temperature was estimated as of about 3000 K.[19]

Physical Chemistry Chemical Physics Accepted Manuscript

PCCP

Cite this: DOI: 10.1039/c0xx00000x

www.rsc.org/xxxxxx

Paper

Table2. Calculated concentration of plasma species at point 0.5 mm above the center of the substrate (z=0.5 mm, r=0). Parameter U(exp/model) corresponds to the measured/calculated discharge voltage. Parameter T corresponds to calculated gas temperature.

Species	Discharge parameters			
	Step S0 P-150 Torr, I-0.7 A U(exp/model)-690/690 V T-1641 K	Step S1 P-150 Torr, I-0.9 A U(exp/model)-690/670 V T-1750 K	Step S2 P-100 Torr, I-0.7 A U(exp/model)-600/580 V T-1374 K	Step S3 P-100 Torr, I-0.9 A U(exp/model)-600/560 V T-1388 K
	Concentration [$\times 10^{14}$ cm^{-3}]			
H	81.2	124	23	28
CH_3	2.45	1.45	4.1	3.3
C_2H_2	219	205	161	173
CH_2	1.9×10^{-2}	2.1×10^{-2}	5.5×10^{-3}	6.7×10^{-3}
CH_2 (singlet)	8.7×10^{-4}	1.1×10^{-3}	2.1×10^{-4}	2.3×10^{-4}
CH	6.9×10^{-4}	1.2×10^{-3}	8×10^{-5}	1.2×10^{-4}
C	9.1×10^{-4}	2.5×10^{-3}	3.7×10^{-5}	7×10^{-5}
C_2	4.3×10^{-5}	9.8×10^{-5}	1.3×10^{-5}	1.3×10^{-5}
C_2(X)	3.2×10^{-6}	1.3×10^{-5}	1.2×10^{-7}	1.8×10^{-7}
C_2H	7.2×10^{-3}	1.8×10^{-2}	5.1×10^{-4}	6.9×10^{-4}
C_2H_3	0.095	0.068	0.089	0.1
C_2H_4	1.44	0.57	3.9	3.6
C_2H_5	6×10^{-4}	1.5×10^{-4}	5.7×10^{-3}	3.5×10^{-3}
C_2H_6	4.2×10^{-3}	5.1×10^{-4}	0.16	0.08
CH_4	13.3	4.81	62.8	41
C_3	0.088	0.16	0.012	0.023
C_3H	2.9×10^{-3}	4.1×10^{-3}	7.4×10^{-4}	1.1×10^{-3}
C_3H_2	2.54	2.22	1.91	2.2
C_4	9.9×10^{-8}	4×10^{-7}	3.5×10^{-9}	5.8×10^{-9}
C_4H	3.2×10^{-5}	7.8×10^{-5}	3.5×10^{-6}	4.6×10^{-6}
C_4H_2	0.61	0.59	0.43	0.5
H(2)	2.4×10^{-6}	4.4×10^{-6}	4×10^{-7}	4.3×10^{-7}
H(3)	1.5×10^{-7}	2.9×10^{-7}	2.7×10^{-8}	2.9×10^{-8}
H_2(1)	277	296	196	185
H_2^*	2.6×10^{-4}	2.9×10^{-4}	1.2×10^{-4}	1×10^{-4}
e	8.6×10^{-3}	1×10^{-2}	4.7×10^{-3}	4.7×10^{-3}
$C_2H_2^+$	8×10^{-3}	9.4×10^{-3}	4.3×10^{-3}	4.4×10^{-3}
$C_2H_3^+$	6.4×10^{-4}	8.9×10^{-4}	3.7×10^{-4}	3.5×10^{-4}
H_3^+	1×10^{-6}	1.4×10^{-6}	5.6×10^{-7}	4.9×10^{-7}
H_2^+	2.3×10^{-8}	2.8×10^{-8}	1.5×10^{-8}	1.2×10^{-8}
H_2	8.5×10^{3}	7.9×10^{3}	6.8×10^{3}	6.7×10^{3}
CH_3/H	0.030	0.012	0.178	0.118

Conclusions

Here we showed that rapid variation of discharge current and/or gas pressure during plasma CVD growth induce nucleation of secondary nanowalls at a CNW surface or promotes hydrogen etching of CNW basal planes. We employed a two-dimensional theoretical model of the plasma to compare radical composition for different discharge parameters. We found that rapid rise in discharge current leads to increase in concentrations of C_xH_y that could chemisorb on basal planes of the CNWs acting as a nucleation sites for the secondary nanowall formation. In turn rapid decrease in gas pressure stimulates hydrogen etching of the CNWs.

Acknowledgments

Authors sincerely acknowledge A. Egorov for support in TEM investigation. Authors also thank HZB for granting of the beam time at BESSY II. This work was financially supported by grantsMK.2773.2014.2. TEM study was supported by the program "Research Priorities in Sciences" at MSU.

Notes and references

[a]*Institute of Nuclear Physics, Moscow State University, Moscow, 119991, Russia, Fax:+7495-939-0909; Tel:+7495-939-4064; E-mail: victi81@mail.ru*

Physical Chemistry Chemical Physics Accepted Manuscript

[b]Department of Chemistry, Moscow State University, Moscow, 119992, Russia
[c] Department of Materials Science, Moscow State University, Moscow, 119992, Russia
[d] Department of Physics, Moscow State University, Moscow, 119992, Russia
[e]Skolkovo Institute of Science and Technology, Skolkovo, 143025 Russia
† Electronic Supplementary Information (ESI) available: [details of any supplementary information available should be included here]. See DOI: 10.1039/b000000x/

1 Victor Krivchenko , Pavel Shevnin , Andrey Pilevsky , Aleksander Egorov , Nikolay Suetin , Vasiliy Sen , Stanislav Evlashin and Aleksander Rakhimov, *J. Mater. Chem.*, 2012, **22**, 16458 – 16464.
2 D. Banerjee, S. Mukherjee, K.K. Chattopadhyay, *Appl. Surf. Sci.*, 2011, **257**, 3717–3722.
3 Boris I Podlovchenko, Victor A Krivchenko, Jury M Maksimov, Tatjana D Dladysheva, Lada V Yashina, Stanislav A Evlashin, Andrej A Pilevsky, Electrochim.Acta, 2012, **76**, 137-144.
4 Victor A. Krivchenko, Daniil M. Itkis, Stanislav A. Evlashin, Dmitry A. Semenenko, Eugene A. Goodilin, Alexander T. Rakhimov, Anton S. Stepanov, Nikolay V. Suetin, Andrey A. Pilevsky, *Carbon*, 2012,**50**, 1422-1444.
5 Hua Wang, Yan Su, Shuo Chen, Xie Quan, *Materials Research Bulletin*, 2013, **48**, 1304–1307.
6 V. A. Krivchenko, S. A. Evlashin, K. V. Mironovich, N. I. Verbitskiy, A. Nefedov, C. Wo¨ll, A. Ya. Kozmenkova, N. V. Suetin, S. E. Svyakhovskiy, D. V. Vyalikh, A. T. Rakhimov, A. V. Egorov and L. V. Yashina, *Sci. Rep.*, 2013, **3**, 3328, 1-6.
7 Y. Wu, P. Qiao, T. Chong and Z. Shen, *Adv. Mater.*, 2002, **14**, 64-67.
8 Zheng Bo, Yong Yang , Junhong Chen, Kehan Yu, Jianhua Yan and Kefa Cen, *Nanoscale*, 2013, **5**, 5180-5204
9 M. Hiramatsu, K. Shiji, H. Amano, M. Hori, *Appl. Phys. Lett*., 2004, **84**, 4708
10 D.H. Seo, A.E. Rider, S. Kumar, L.K. Randeniya, K. Ostrikov, *Carbon*, 2013, **60**, 221-228
11 V. A. Krivchenko, V. V. Dvorkin, N. N. Dzbanovsky, M. A. Timofeyev, A. S. Stepanov, A. T. Rakhimov, N. V. Suetin, O.Vilkov and L. V. Yashina,*Carbon*, 2012,**50**, 1477-1487.
12 Zhu M, Wang J, Holloway BC, Outlaw RA, Zhao X, Hou K,*Carbon*, 2007,**45**, 2229–34.
13 Malesevic A, Vitchev R, Schouteden K, Volodin A, Zhang L, Van Tendeloo G, *Nanotechnology*, 2008,**19**, 305604-1-6.
14 K. Ostrikov, E.C. Neyts, M. Meyyappan, *Adv.Phys.*, 2013, **62**, 113-224.
15 Jiong Zhao, Mehrdad Shaygan, Jurgen Eckert,M. Meyyappan,Mark H. Rummeli, *Nano Lett.,* 2011, **49**, 3064-3071.
16 D.H. Seo, S. Kumar, K. Ostrikov, *Carbon*, 2011, **49**, 4331-4339.
17 Hironao Shimoeda, Hiroki Kondo, Kenji Ishikawa, Mineo Hiramatsu, Makoto Sekine, Masaru Hori, *Appl. Phys. Express*, 2014, **7**, 046201.
18 R.W.B Pearse, A.G. Gaydon, Chapman and Hall, London, 1963, 3rd edition.
19 Ma J., Richley J.C., Ashfold M.N.R, Mankelevich Yu.A. , *J. Appl. Phys.*, 2008, **104**, 103305.
20 Kostiuk S.V., Mankelevich Y.A., Rakhimov A.T., Suetin N.V., *Proc. of Physics and Technology Institute*, 2000,**16**, 38-47.
21 Mankelevich Yu.A., Ashfold M.N.R., Ma J., *J. Appl. Phys.,*2008,**104**, 113304.
22 L.M.Malard, M.A.Pimenta, G.Dresselhaus, M.S.Dresselhaus, *PhysicsReports*, 2009, **473**, 51-87.
23 Axel Eckmann, Alexandre Felten, Artem Mishchenko, Liam Britnell, Ralph Krupke, Kostya S. Novoselov, and Cinzia Casiraghi, *Nano Lett.*, 2012, ***12*** , 3925–3930.
24 Axel Eckmann, Alexandre Felten, Ivan Verzhbitskiy, Rebecca Davey and Cinzia Casiraghi, *Rhys.Rev.B*, 2013,**88**, 035426.
25 Fengting T. Wang, Lei Chen, Chua njin J. Tian, Yan Meng, Zhi gang G. Wang, Ruiqin Q. Zhang, Mingxing X. Jin, Ping Zhang, and Dajun J. Ding, *J. Comput. Chem*., 2011, **32**, 3264-3268
26 Rong Yang, Lianchang Zhang, Yi Wang, Zhiwen Shi, Dongxia Shi, Hongjun Gao, Enge Wang and Guangyu Zhang, *Adv. Mater*., 2010, **22**, 4014–4019.
27 C. Kanai, K. Watanabe and Y. Takakuwa, *Phys. Rev.B*, 2001, **63**, 235311.
28 Chong Wang, Bo Xiao, and Yi-hong Ding, *ChemPhysChem,* 2012, **13**, 774 – 779.

Physical Chemistry Chemical Physics Accepted Manuscript